ADVANCED MATERIALS
www.advmat.de

Materials Views
www.MaterialsViews.com

A Facile and General Approach for the Direct Fabrication of 3D, Vertically Aligned Carbon Nanotube Array/Transition Metal Oxide Composites as Non-Pt Catalysts for Oxygen Reduction Reactions

Zhi Yang, Xuemei Zhou, Zhiping Jin, Zheng Liu, Huagui Nie, Xi'an Chen, and Shaoming Huang**

In recent years, ever-increasing energy demands have driven the development of energy storage devices (ESDs) with higher power and energy densities;[1] these devices meet the requirements for applications such as cordless electric tools, hybrid electric vehicles, and industrial energy management. Because of their environmentally friendly nature, safety, low cost, and good electrochemical performance, transition-metal oxides (MOs) have been widely studied in many energy fields as electrocatalysts for oxygen reduction reactions (ORRs),[2] and as electrode materials for lithium-ion batteries[3] and supercapacitors.[4] However, their poor conductivity has limited their practical application in electrochemical devices. One promising approach to address this problem is the incorporation of MOs into electric carbon nanomaterials such as carbon black, carbon nanotubes (CNTs), and graphene.[5] In recent years, it has been widely demonstrated that introducing CNTs into MOs can increase their electrochemical performance.[6] However, the improved performance produced by the simplex incorporation between the one-dimensional (1D) CNTs and the MOs is still too limited to meet the requirements described above.[1] It is known that ionic and electronic transport lies at the heart of energy storage and conversion systems in ESDs, and it is widely accepted that it will play a vital role in achieving ideal electrochemical performance.[7] Therefore, in this sense, the design of architectures that can provide highly efficient ionic and electronic transport is of both scientific and practical significance. Three-dimensional (3D) carbon-based nanostructures, particularly vertically aligned carbon nanotube arrays (VACNTs), may present an ideal architecture, because of their well-directed 1D conductive electron paths, as well as an appropriate inter-tube spacing that can ensure the highly efficient transport of electrolytic ions and intermediate reactants.[1,8] Considering the characteristics of MOs and the advantages of VACNTs, it would seem highly desirable to combine 3D VACNTs and MOs to achieve certain exciting functions, especially in the electrochemical fields.

To achieve the uniform and deep decoration of MOs on VACNTs, three practical problems must be addressed: (1) VACNTs typically have a high density of CNTs, and the resulting limited inter-tube spacing may be unfavorable for the embedding of MOs; (2) CNTs' intrinsic hydrophobicity prevents aqueous solutions from entering the internal spaces of VACNTs; and (3) the processes used for the growth and compositing of VACNTs are typically carried out in different environments, and VACNTs must therefore be transferred from the growth substrate to a second substrate. Considering the high fragility of VACNTs, this transfer process is likely to be damaging to the quality of the VACNTs. Recently, a few researchers have attempted to fabricate 3D VACNTs decorated with various MOs (such as MnO_2, NiO, and ZnO), using electrochemical deposition,[4,9,10] atomic layer deposition,[11] and microwave-assisted techniques.[12] As electrode materials, these 3D structures also exhibited superior performance in super-capacitor or Li-ion battery applications. However, these previous studies only touched on one or two of the three practical problems detailed above,[4,9–12] thus progress seems to be limited and 3D composite-based VACNTs are still far from showing the desired performance. To the best of our knowledge, so far it is still considered a challenging task to obtain the high-quality 3D structure-based VACNTs decorated MO.

In this study, after comprehensively considering the three practical problems described above, we introduced a new strategy involving nebulized ethanol assisted infiltration for the fabrication of 3D structure-based VACNTs uniformly decorated with MOs. As illustrated in **Figure 1**, the method can be divided into a simple three-step process. In the first step, VACNTs are synthesized using the nebulized spray pyrolysis of ferrocene/xylene solutions at high temperature.[13] The number density of CNTs in the VACNTs was adjusted by varying the concentration of ferrocene in the xylene solution. In the second step, the ethanol solutions containing the MO precursors were nebulized to generate a mist of droplets, and the resulting droplets were infiltrated into the inter-tube spaces in the VACNTs at 75 °C, using an N_2 carrying gas. The nebulization action coupled with ethanol evaporation significantly decreased the size of the droplets, and was helpful for the uniform and deep infiltration of the MO precursors into the VACNTs. More importantly, the Video 1 and 2 in Supporting Information S1 showed that the penetration of the ethanol into the VACNT films was far superior to that of the aqueous solution. The results suggested that using ethanol containing MO precursors instead of

Dr. Z. Yang, X. Zhou, Z. Jin, Z. Liu, H. Nie,
X. Chen, Prof. S. Huang
Nanomaterials & Chemistry Key Laboratory
Wenzhou University
Wenzhou 325027, China
E-mail: yang201079@126.com; smhuang@wzu.edu.cn

DOI: 10.1002/adma.201305513

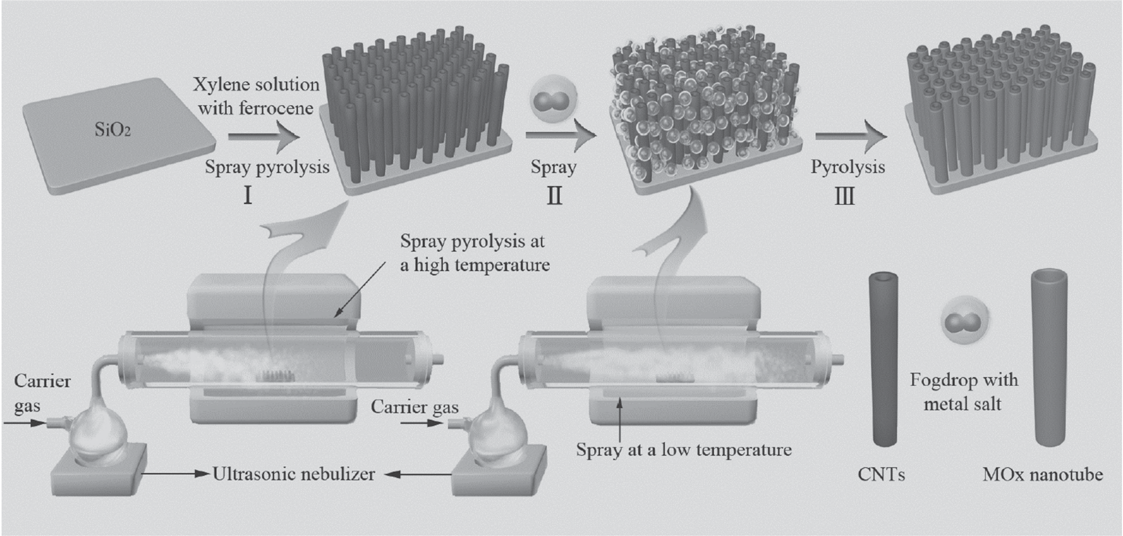

Figure 1. Schematic diagram showing the fabrication of 3D structure-based VACNTs decorated with various MOs.

aqueous solutions represented an ideal strategy for achieving the uniform and deep decoration of MOs on VACNTs. To the best of our knowledge, this strategy involving nebulized ethanol assisted infiltration has not been proposed in any previous reports. In the third step, MO nanoparticles were easily formed in the VACNTs via the pyrolysis reaction of the MO precursors at high temperature. Our strategy to fabricate the 3D structures holds several advantages, as follows: First, the VACNTs stand on the same quartz slice for the entire experimental process, and the transfer of VACNTs is thus avoided; this is advantageous in ensuring the quality of the 3D structure. Second, with the help of both the ethanol-assisted infiltration and the nebulizing action, the uniform and deep decoration of MOs into the VACNTs is easily achieved. The decorated deepness can reach several hundred micrometers. So far there are few reports on the functionalization of the 100 μm level and above thick VACNTs.[10] Third, this simple approach can be generally applied for the decoration of various MOs (e.g., MnO_2, ZnO, NiO, Fe_3O_4, and TiO_2) into VACNTs. These high-quality, 3D structure-based VACNTs uniformly decorated with various MOs could have significant applications in energy generation or storage, and in the optoelectronics field.

Figures 2 and S2 illustrate the morphological characterization of the VACNTs and the 3D structure-based VACNTs decorated with MnO_2. From the low-magnification scanning electron microscope (SEM) image in Figure S2a, it can be seen that large-area, aligned CNT forests were successfully synthesized via the nebulized spray pyrolysis method. The relatively high-magnification SEM images (Figure 2a and b) clearly show that the VACNTs obtained using a ferrocene concentration of 18 g/L had good alignment, a thickness of ~200 μm, an average outer diameter of ~50 nm, and an inter-tube distance of ~200 nm. Figure 2c, d, e, f and g show SEM images of the 3D structures. As shown in Figure 2c and d, the VACNTs decorated with MnO_2 still exhibited good alignment. The typical higher magnification SEM images (Figure 2e, h and g) show that the MnO_2 particles were uniformly and deeply deposited on the VACNTs. The MnO_2 loading mainly depended on the duration of the nebulization action in the second step described above; the loading was analyzed using inductively coupled plasma-atom emission spectroscopy, and loading values of 10.3, 19.6, and 27.8 wt% were measured for the samples obtained using nebulization times of 5, 10, and 20 min, respectively. The STEM and the corresponding elemental mapping images (Figure 2h) further confirmed the uniform decoration of MnO_2 particles on the VACNTs. From the transmission electron microscope (TEM) image in Figure 2i, it can be seen that the diameter of the MnO_2-decorated VACNTs reached ~80 nm, compared with the as-grown diameter of the VACNTs (50 nm). Interestingly, no clear interface was observed in the TEM image between the VACNTs and the MnO_2. Furthermore, in our previous report,[2] it has been confirmed that the spontaneous electron transfer between CNTs and MnO_2 can occur when MnO_2 materials are directly coated on CNTs. Some recent reports also support our results.[14] Thus it is believed that the close interface link between the VACNT and MnO_2 may be beneficial to achieve the highly effective electron transfer and the excellent synergistic effects between these materials. The high-resolution TEM image in the upper right of Figure 2i showed a typical lattice fringe, which clearly revealed an inter-planar distance of approximately 0.241 nm, corresponding to the spacing between two (101) planes of MnO_2. As shown in Figure S3, the X-ray diffraction (XRD) pattern for the MnO_2-decorated VACNTs displayed four typical peaks (37.4, 42.9, 43.6 and 44.8°) of MnO_2, which were attributed to the (101), (111), (401), and (321) planes, respectively. The XRD results further confirmed the presence of MnO_2 on the VACNTs, and were consistent with the HRTEM observations. As described above, high-quality, 3D structure-based VACNTs uniformly and deeply decorated with MnO_2 were obtained using the simple three-step method.

Recently, it has been confirmed that MnO_2/VACNT composites exhibit superior performance in super-capacitor or Li-ion battery applications,[3,4] and the hybrids of VACNTs decorated with other particles such as C-N-Fe[15] and Fe[16] have been developed as ORR catalysts, but research into 3D structure-based VACNTs decorated with MnO_2 for cathode catalysts in

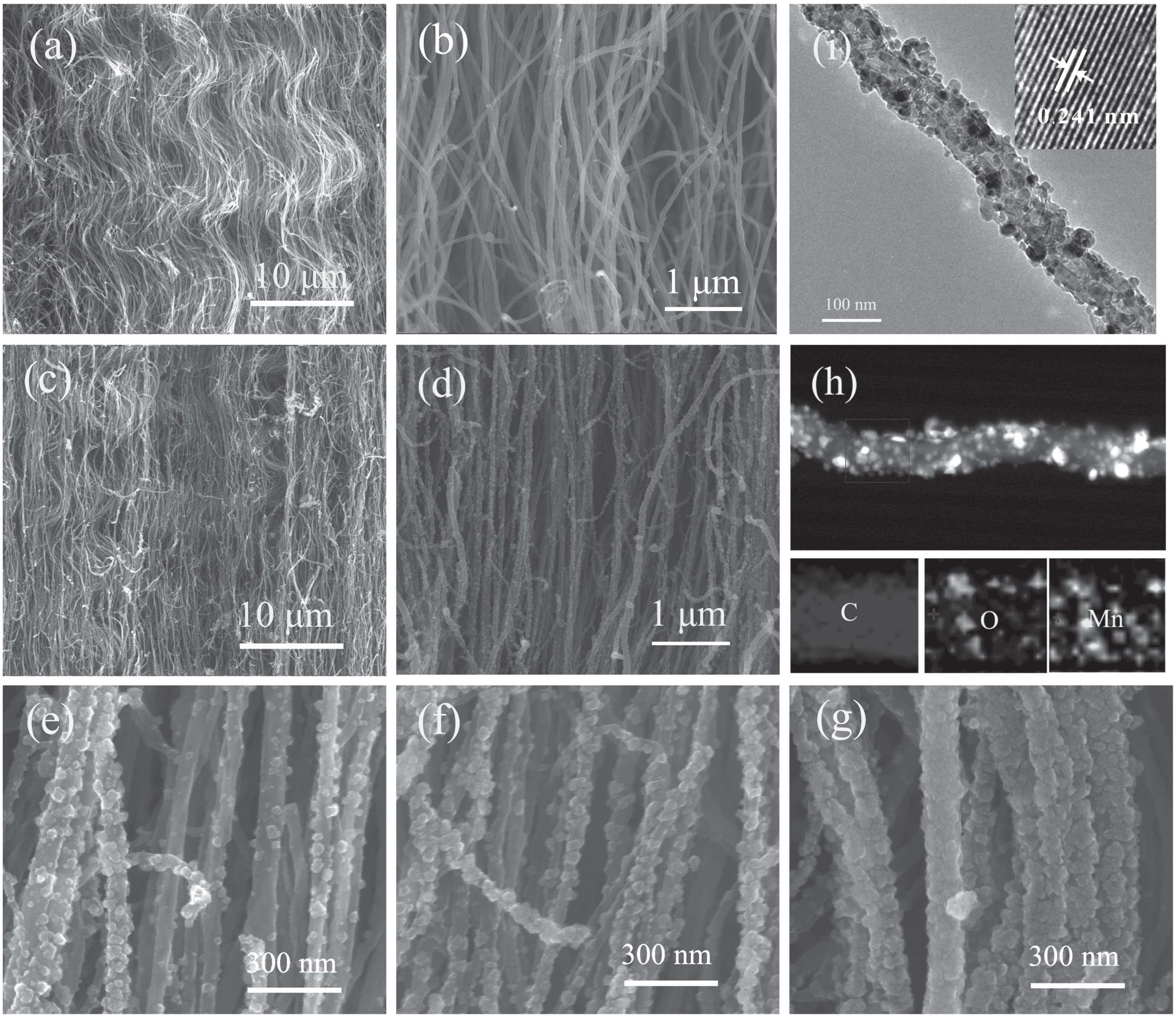

Figure 2. Typical SEM, STEM elemental mapping and TEM images of (a, b) ACNTs and the resulting VACNTs-MnO_2 composites obtained using different nebulization time: (e) 5 min, (c,d, f, h, i) 10 min and (g) 20 min.

fuel cells is rare. It is clear that the advantages of these 3D structures could also be beneficial for promoting ORRs. To evaluate the electrocatalytic ORR activity of these 3D structures, cyclic voltammetry (CV) measurements were carried out in a 0.1 M KOH solution. **Figure 3**a shows the ORR peaks for the VACNTs and the 3D structures obtained using different nebulization times under O_2-saturated conditions. Their physical parameters, electrochemical properties, and corresponding experimental data are listed in Table S1. For the VACNT electrode, a single cathodic reduction peak was present at –0.38 V (vs Ag/AgCl). After the combination with MnO_2, the VACNTs-MnO_2–1 and VACNTs-MnO_2–2 electrodes showed higher peak currents and more positive peak potentials than the VACNT electrode. These experimental results indicated that the decoration of MO on the VACNTs was highly effective in enhancing the activity and reducing the overpotentials toward ORRs. Furthermore, from Figure 3a, it can also be seen that VACNT-MnO_2–2 showed the highest peak current of all of the samples. When the nebulization time was increased beyond 10 min, the ORR activity (for the VACNTs-MnO_2–3 sample) decreased. This might have been due to the comparatively high MnO_2 content, which could have resulted in a decrease in the interfacial area between the CNTs and the electrolyte, thus increasing the resistance compared with the VACNTs-MnO_2 electrode. To gain further insights into the ORR performance of these samples, we also performed linear sweep voltammetry measurements on a rotating-disk electrode (RDE) using a rotation rate of 1600 rpm, and the results were compared with those obtained using a commercial Pt/C catalyst (20 wt%). From Figure 3b, it can be seen that the VACNT-MnO_2–1 and VACNT-MnO_2–2 samples had higher limiting current densities than the VACNTs. This result further supported the CV observations described above, and strongly indicated that the introduction of MnO_2 enhanced the ORR catalytic activity. Furthermore, from Figure 3b, we can also observe that the onset potential for VACNTs-MnO_2–2 was close to that of the Pt/C catalyst, and that its current density

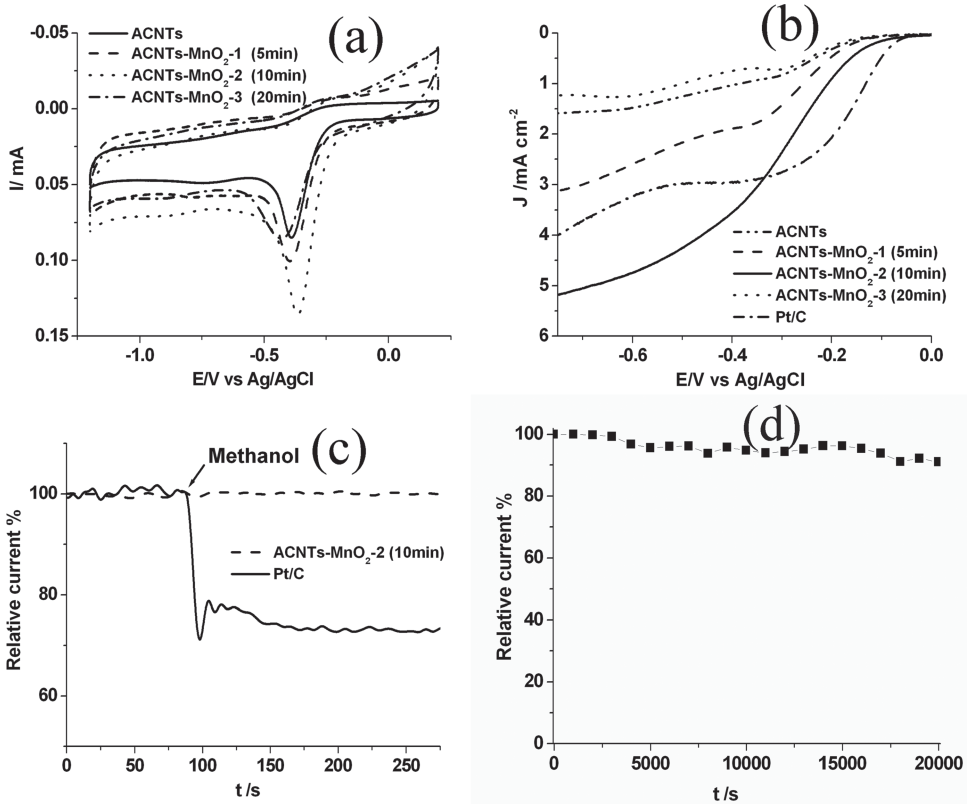

Figure 3. (a) CVs for ACNTs and the resulting VACNTs-MnO$_2$ composites obtained using different nebulization time, (b) LSV curves for various catalysts and a Pt/C catalyst at a rotation rate of 1600 rpm, chronoamperometric responses of VACNTs-MnO$_2$–2 and Pt/C catalyst, (c) with 3 M methanol added at around 80 s, and (d) at –0.40 V in an O$_2$-saturated 0.1 M KOH solution.

was higher than that of the Pt/C catalyst. These results suggested that the ORR catalytic activity of VACNTs-MnO$_2$–2 was better than that of commercial Pt/C catalysts. Considering its physical parameters (Table S1) and morphological character, it is believed that the excellent performance observed for the VACNTs-MnO$_2$–2 sample can be attributed to the good synergistic effects between the VACNTs and MnO$_2$, and that the 3D structures ensured the highly efficient transport of electron, electrolytic ions and intermediate reactants. To further confirm the role of VACNTs-MnO$_2$–2 in the ORR electrochemical process, we also performed RDE measurements at various rotation speeds (See Figure S4). The number of electron transfers for VACNTs-MnO$_2$–2 was calculated to be 3.83, which indicated a four-electron-transfer reaction. The calculated limited-kinetics current density (J_k) was 19.82 mA cm^{-2} at –0.45 V. The electrocatalytic activity of VACNT-MnO$_2$–2 was comparable to that of other non-Pt catalysts (e.g., Co$_3$O$_4$/N-graphene, S (or Se)-doped graphene and mesoporous graphitic arrays)[17–20] in alkaline electrolytes. The above results further confirmed that VACNTs-MnO$_2$–2 is a promising non-Pt material with high catalytic activity for ORRs.

Possible crossover effects and the stability of the catalyst materials are both important parameters for the evaluation of their practical application in fuel cells. Therefore, the chronoamperometric responses to methanol introduced into an O$_2$-saturated electrolyte were measured for both VACNTs-MnO$_2$–2 and a commercial Pt/C catalyst. It can be seen from Figure 3c that after the addition of 3 M of methanol at 80 s, no noticeable change was observed in the ORR current at the VACNTs-MnO$_2$–2 electrode. In contrast, the ORR current for the Pt/C catalyst decreased sharply. These results indicated that VACNTs-MnO$_2$–2 exhibited high ORR selectivity, and had a good ability for avoiding crossover effects. The durability of the VACNTs-MnO$_2$–2 catalysts was also tested by holding them at –0.40 V for 6 h in an O$_2$-saturated 0.1 M KOH solution. Figure 3d shows that the resulting chronoamperometric response for VACNTs-MnO$_2$–2 exhibited a very slow attenuation, and a high relative current of 92.6% that still persisted after 20 000 s. The stability of the VACNTs-MnO$_2$–2 is comparable to that of the previously reported non-Pt ORR catalysts (e.g., nitrogen-doped ordered mesoporous graphitic arrays).[21] These results confirmed that VACNTs-MnO$_2$–2 has the potential to be applied in direct methanol and alkaline fuel cells.

To further test the general applicability of the simple three-step process, other ethanol solutions containing various metal salts (including zinc acetylacetonate hydrate, nickel(II) acetylacetonate, iron(III) acetylacetonate, and titanium tetrachloride) were used as precursors in similar experiments. In these experiments, the ethanol solutions containing different precursors were first nebulized, and the resulting small droplets were infiltrated into the VACNTs using an N$_2$ carrying gas; finally, the resulting samples were heated to various temperatures from 400 to 550 °C, depending on the decomposition temperature of the respective salts. It is known that the thermal decomposition

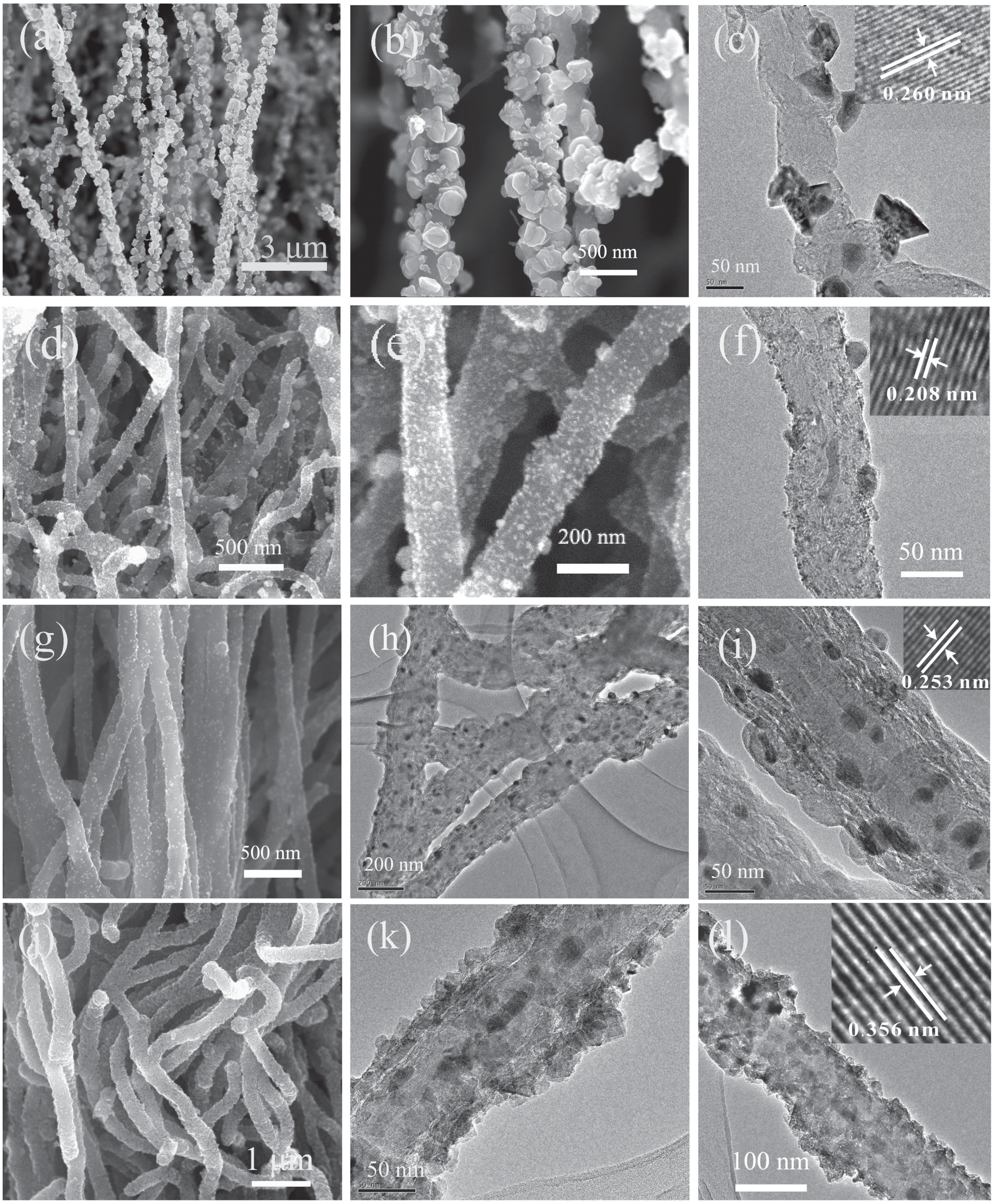

Figure 4. Typical SEM and TEM images of these 3D structure-based VACNTs uniformly decorated with various MOs:(a, b, c) VACNTs-ZnO, (d, e, f) VACNTs-NiO, (g, h, i), VACNTs-Fe_3O_4, and (j, k, l) VACNTs-TiO_2

of these organic salts typically yields the corresponding metal oxide.[21] **Figure 4**, S5, S6, S7 and S8 show typical FESEM, TEM, STEM and corresponding elemental mapping images, and EDX patterns of these 3D structure-based VACNTs uniformly decorated with various MOs (ZnO, NiO, Fe_3O_4, and TiO_2). As an example, Figure 4a-c and S5 show that ZnO particles with a narrow size distribution were uniformly decorated on the VACNTs, with the help of both the ethanol-assisted infiltration and the nebulization. These novel 3D structure-based VACNTs decorated with ZnO (VACNTs-ZnO) may hold advantages for applications in dye-sensitized solar cells, gas sensors, and piezoelectric devices. Furthermore, considering Figure 4d–l, S6, S7 and S8, it is interesting to note that the other MO particles could also achieve uniform and deep decoration on the VACNTs, but there were slight differences for the different MOs. NiO, Fe_3O_4, and TiO_2 appeared as individual nanoparticles with small sizes on the order of several nanometers, while ZnO tended to form clusters of relatively large nanoparticles on the surfaces of VACNTs under the experimental conditions used in this study. This difference might have originated from the different crystallization and crystal growth behavior of the different materials during the annealing process. The detailed decomposition mechanisms for these different metal salts must be studied further.

In summary, we have developed a simple and effective strategy for the general synthesis of 3D structure-based VACNTs uniformly decorated with MOs. Using this method, various MO precursors can be uniformly and deeply infiltrated into VACNTs with the help of both ethanol-assisted infiltration and nebulization, finally achieving the formation of high-quality 3D structures after thermal annealing. The facile nature, versatility, and scalability of this method mean that it has great potential for the preparation of other metal oxide nanoparticle decorated carbon materials and other nanostructures for catalytic, electronic, and optical applications. Furthermore, we have also demonstrated that the 3D structure-based VACNTs uniformly decorated with MnO_2 exhibit superior electrocatalytic activity, long-term stability, and an excellent resistance to crossover effects for ORRs. The materials are ideal potential candidates for replacing Pt-based catalysts as cathodes in fuel cells.

Supporting Information

Supporting Information is available from the Wiley Online Library or from the author.

Acknowledgements

The work was supported in part by grants from NSFC (51002106, 21273163, 21005055, 21173259) and NSFC for Distinguished Young Scholars (51025207), ZJST (2012R10014–08), NSFZJ (LY13B050002) and ZJED Innovative Team for S. Huang.

Received: November 5, 2013
Revised: December 14, 2013

[1] H. Jiang, P. S. Lee, C. Z. Li, *Energy Environ. Sci.* **2013**, *6*, 41–53.
[2] Z. Yang, X. M. Zhou, H. G. Nie, Z. Yao, S. M. Huang, *ACS Appl. Mater. Inter.* **2011**, *3*, 2601.
[3] A. L. Mohana Reddy, M. M. Shaijumon, S. R. Gowda, P. M. Ajayan, *Nano Lett.* **2009**, *9*, 1002.
[4] J. W. Liu, J. Essner, J. Li, *Chem. Mater.* **2010**, *22*, 5022.
[5] Y. Hou, Y. W. Cheng, T. Hobson, J. Liu, *Nano Lett.* **2010**, *10*, 2727.
[6] S. W. Lee, J. Kim, S. Chen, P. T. Hammond, Y. Shao-Horn, *ACS Nano* **2010**, *4*, 3889.
[7] M. J. Nanoionics, *Nat. Mater.* **2005**, *4*, 805.
[8] K. P. Gong, F. Du, Z. H. Xia, M. Durstock, L. M. Dai, *Science* **2009**, *323*, 760.
[9] H. Zhang, G. P. Cao, Z. Y. Wang, Y. S. Yang, Z. J. Shi, Z. N. Gu, *Nano Lett.* **2009**, *8*, 2664.
[10] Y. Q. Jiang, P. B. Wang, X. N. Zang, Y. Yang, A. Kozinda, L. W. Lin, *Nano Lett.* **2013**, *13*, 3524.
[11] C. J. Hu, Y. H. Lin, C. W. Tang, M. Y. Tsai, W. K. Hsu, H. F. Kuo, *Adv. Mater.* **2011**, *23*, 941.
[12] M. Mazloumi, S. Shadmehr, Y. Rangom, L. F. Nazar, X. W. Tang, *ACS Nano* **2013**, *7*, 4281.
[13] Z. Yang, X. H. Chen, H. G. Nie, K. Zhang, W. H. Li, B. Yi, *Nanotechnology* **2008**, *19*, 5606.
[14] Y. Y. Liang, Y. G. Li, H. L. Wang, H. J. Dai, *JACS* **2013**, *135*, 2013.
[15] G. C. K. Liu, J. R. Dahn, *Applied Catalysis A: General* **2008**, *347*, 43.
[16] H. Chung, J. H. Won, P. Zelenay, *Nat. Commu.* **2013**, *4*, 1992.
[17] Y. Y. Liang, Y. G. Li, H. L. Wang, J. G. Zhou, J. Wang, T. Regier, H. J. Dai, *Nat. Mater.* **2011**, *10*, 780.
[18] Z. Yang, Z. Yao, G. Y. Fang, G. F. Li, H. G. Nie, X. M. Zhou, X. Chen, S. M. Huang, *ACS Nano* **2012**, *6*, 205.
[19] Z. P. Jin, H. G. Nie, Z. Yang, J. Zhang, Z. Liu, X. J. Xu, S. M. Huang, *Nanoscale* **2012**, *4*, 6455.
[20] R. L. Liu, D. Q. Wu, X. L. Feng, K. Mullen, *Angew. Chem. Int. Ed.* **2010**, *49*, 2565.
[21] V. Logvinenko, O. Polunina, Y. Mikhailov, K. Mikhailov, B. Bokhonov, *J. Therm. Anal. Calorim.* **2007**, *90*, 813.